Light trapping in thin-film solar cells via scattering by nanostructured antireflection coatings

X. H. Li, P. C. Li, D. Z. Hu, D. M. Schaadt, and E. T. Yu

Citation: Journal of Applied Physics **114**, 044310 (2013); doi: 10.1063/1.4816782
View online: http://dx.doi.org/10.1063/1.4816782
View Table of Contents: http://scitation.aip.org/content/aip/journal/jap/114/4?ver=pdfcov
Published by the AIP Publishing

Light trapping in thin-film solar cells via scattering by nanostructured antireflection coatings

X. H. Li,[1] P. C. Li,[1] D. Z. Hu,[2,3] D. M. Schaadt,[2,3] and E. T. Yu[1]
[1]*Microelectronics Research Center, University of Texas at Austin, 10100 Burnet Rd., Austin, Texas 78758, USA*
[2]*Clausthal Technical University, Institute of Energy Research and Physical Technologies, Clausthal, Germany*
[3]*Energy Center of Lower Saxony, Germany*

(Received 12 June 2013; accepted 12 July 2013; published online 25 July 2013)

The use of nanostructured TiO_2 layers fabricated on thin-film solar cells to provide, simultaneously, both antireflection functionality and light trapping via scattering of long-wavelength photons into guided optical modes is demonstrated and analyzed in thin-film quantum-well solar cells. Nanosphere lithography is used for fabrication of periodic arrays of subwavelength-scale TiO_2 structures, and separation of active device layers from their epitaxial growth substrate and integration with the nanostructured TiO_2 layer enables increased optical absorption via coupling to both Fabry-Perot resonances and guided lateral propagation modes in the semiconductor. The nanostructured TiO_2 layer is shown to act as a graded-index coating at optical wavelengths and simultaneously to scatter incident light into guided optical modes within the device. The dependence of these effects on angle of incidence is also analyzed. © *2013 AIP Publishing LLC*. [http://dx.doi.org/10.1063/1.4816782]

I. INTRODUCTION

A variety of approaches for exploiting subwavelength-scale metal and dielectric structures to induce light trapping and increased optical absorption in thin-film solar cells have emerged in recent years.[1–8] For optimal overall device performance, the structures required for light trapping must generally be integrated with antireflection coatings present on the top surface of the solar cell and this can severely constrain the incorporation of light trapping structures on the top surface of a thin-film photovoltaic device. However, the advent of nanostructured antireflection coatings, which can provide broad-spectrum, wide-angle antireflection functionality,[9–14] offers an opportunity to achieve both antireflection and light trapping (scattering) functionality simultaneously with a single, appropriately designed, nanostructured layer at the device surface.

In this paper, we demonstrate and analyze the use of subwavelength-scale TiO_2 nanostructures fabricated on thin-film quantum-well solar cells to provide both antireflection performance superior to that of a single-layer antireflection coating, e.g., a silicon nitride thin film, and, when combined with a substrate removal process that enables the entire solar cell device to act as a thin-film waveguide,[15] light trapping within the solar cell that substantially improves short-circuit current density. While the basic concepts demonstrated are applicable to any thin-film solar cell, their use in quantum-well solar cells allows long-wavelength light-trapping effects to be demonstrated and analyzed more clearly than in a conventional pn homojunction cell due to the extended range of wavelengths for which optical absorption occurs only in the quantum wells.

II. EXPERIMENT

Samples were grown by solid-source molecular beam epitaxy (MBE) on GaAs (001) n-type substrates with the structure shown schematically in Figure 1(a). A 300 nm n-type ($n \sim 2.5 \times 10^{18}\,cm^{-3}$) $Al_{0.85}Ga_{0.15}As$ sacrificial etch stop layer was grown initially, followed by a 200 nm n-type ($n \sim 2.0 \times 10^{18}\,cm^{-3}$) GaAs layer. An unintentionally doped layer was then grown consisting of three 4 nm $In_{0.30}Ga_{0.70}As$ quantum wells separated by 17 nm GaAs barriers with 21 nm undoped GaAs layers immediately above and below the quantum-well region. A 1500 nm p-type (Be-doped, $p \sim 5 \times 10^{18}\,cm^{-3}$) GaAs layer and finally a 20 nm p^+ ($p \sim 5 \times 10^{19}\,cm^{-3}$) GaAs contact layer then completed each epitaxial layer structure. The growth temperature was kept above 500 °C throughout.

Final device structures, shown schematically in Figures 1(b)–1(d), were fabricated using processes illustrated schematically in Figure 2(a). First, 10 nmCr/100 nm Au/1200 nm In metallization was deposited on the p^+ GaAs surface. The top In layer was then bonded to a Si (001) wafer on which 10 nm Ti/800 nm Au had been deposited by pressing the metalized surfaces together at 180 °C for 20 min in a home-built wafer-bonding apparatus, leading to formation of a robust Au/In bonding alloy layer.[16] After bonding, the GaAs substrate was removed by chemical etching in $NH_4OH:H_2O_2$ (1:19) followed by 50% citric acid:H_2O_2 (4:1).[17] The edges of the epitaxial wafer were covered with black wax to prevent etching of the active device layers, and the $NH_4OH:H_2O_2$ and citric acid:H_2O_2 etch solution compositions were chosen to maximize the etch rate of the GaAs substrate and the selectivity between the $Al_{0.85}Ga_{0.15}As$ etch stop layer and GaAs device layers, respectively.[6,15] The $Al_{0.85}Ga_{0.15}As$ sacrificial etch stop layer was then removed by etching in 10% dilute hydrofluoric acid, and 1 mm × 1 mm device mesas were fabricated by photolithography and wet etching in $NH_4OH:H_2O_2$ (1:19).

For devices with a conventional single-layer antireflection coating, 76 nm silicon nitride was then deposited on the device surface by e-beam evaporation, and deposition and patterning of 25 nm AuGe/10 nm Ni/100 nm Au n-type Ohmic contact metallization completed the device

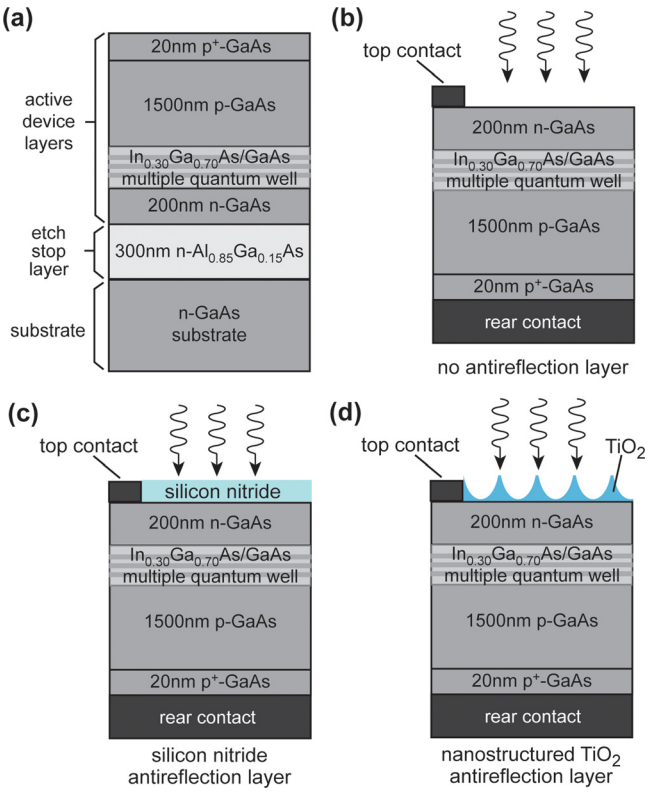

FIG. 1. (a) Schematic diagram of epitaxial layer structures for $In_{0.30}Ga_{0.70}As/GaAs$ quantum-well solar cell structure. Active device layers, etch stop layers, and substrate/buffer layers labeled for each correspond to similarly labeled sample layers in Figure 2. (b)–(d) Schematic diagrams of final quantum-well solar cell device structures fabricated without antireflection layer (b), with silicon nitride thin-film antireflection coating (c), and nanostructured TiO_2 antireflection layer (d).

fabrication process. For devices with a nanostructured TiO_2 antireflection coating, a nanosphere lithography process[18] was employed in which 500 nm diameter polystyrene spheres were deposited on the SiO_2 surface in a monolayer-thick hexagonal array using a Langmuir-Blodgett process.[19] A 250 nm TiO_2 layer was then deposited by e-beam evaporation, followed by a liftoff process performed in toluene with sonication for 3 s to remove the polystyrene spheres, and then the same n-type Ohmic contact metallization process as described above. Figure 2(b) shows scanning electron micrographs of the resulting TiO_2 structures formed on the GaAs surface.

Current-voltage characteristics were measured using normally incident light from a Newport Oriel 96000 solar simulator operating at 150 W with an airmass (AM) 1.5G filter. Photocurrent response spectra were measured at zero bias using a single grating monochromator based system from Optronic Laboratories with AC lock in detection. Numerical simulations of electromagnetic field distributions were performed using the RSOFT DIFFRACTMOD software package (Rsoft Design Group, Inc., Ossining, NY, USA) and standard literature values for optical constants.[20] Incident light was assumed to be in the form of a plane wave normally incident on the device surface. A simulated absorption spectrum $A(\lambda)$ was computed assuming that optical absorption is proportional to the square of the electric field amplitude, and the simulated external quantum efficiency was computed assuming 100% efficiency in photogenerated carrier collection.[21] The simulated short-circuit current density, $J_{sc,th}$, computed for AM1.5G incident illumination, is then given by

$$J_{sc,th} = e\int A(\lambda)I_{AM1.5}(\lambda)d\lambda, \quad (1)$$

where e is the electron charge magnitude, and $I_{AM1.5}(\lambda)$ is the AM1.5G photon flux density.

III. RESULTS AND DISCUSSION

Figure 3(a) shows current-voltage characteristics measured under AM1.5G illumination from a solar simulator for the device structures shown schematically in Figures 1(b)–1(d). As expected, both the single-layer silicon nitride and the nanostructured TiO_2 antireflection layers yield much higher short-circuit current density, J_{sc}—13.82 mA/cm^2 and 14.62 mA/cm^2, respectively—compared to a reference device with no antireflection coating (9.52 mA/cm^2). The difference in J_{sc} between devices with the single-layer silicon nitride and nanostructured TiO_2 antireflection layers arises from a combination of the superior antireflection performance of the latter, especially at shorter wavelengths, and the scattering of light into guided optical modes by the TiO_2 nanostructures on the surface at longer wavelengths, particularly those for which absorption occurs primarily in the $In_{0.30}Ga_{0.70}As$ quantum wells. The superior antireflective properties of the nanostructured TiO_2 layer, compared to those of the silicon nitride thin film coating, are to be expected, as the shape of the TiO_2 structures shown in Figure 2(b) leads to a gradual change in effective refractive index from that of air to that at the semiconductor surface. This type of geometry is well known to allow low surface reflectivity to be achieved over a broad range of wavelengths and to persist over a wide range of incident angles and polarizations.[22–24] What has not been explored, and is shown here, is that the TiO_2 nanostructure array also leads to light trapping via scattering of light into guided optical modes within the solar cell that significantly increases optical absorption efficiency at long wavelengths.

Figure 3(b) shows external quantum efficiency (E.Q.E.) measured experimentally and simulated numerically for the same set of device structures. In the measured spectra, the device with no antireflection coating exhibits, as expected, much lower E.Q.E. at wavelengths longer than the GaAs absorption edge at ~900 nm. At wavelengths shorter than ~600 nm, the measured E.Q.E. is significantly higher for the device with a nanostructured TiO_2 antireflection coating than for that with the single-layer silicon nitride coating, as expected from the simulated E.Q.E. spectra shown in Figure 3(b). At wavelengths longer than ~820 nm, peaks in the measured E.Q.E. spectra are observed for all three device types, and as described below these are associated with Fabry-Perot resonances (in all device types) and scattering of light into guided modes within the semiconductor layer (with the nanostructured TiO_2 antireflection layer). For wavelengths between ~600 nm and ~820 nm, devices with each type of antireflection coating exhibit very similar measured

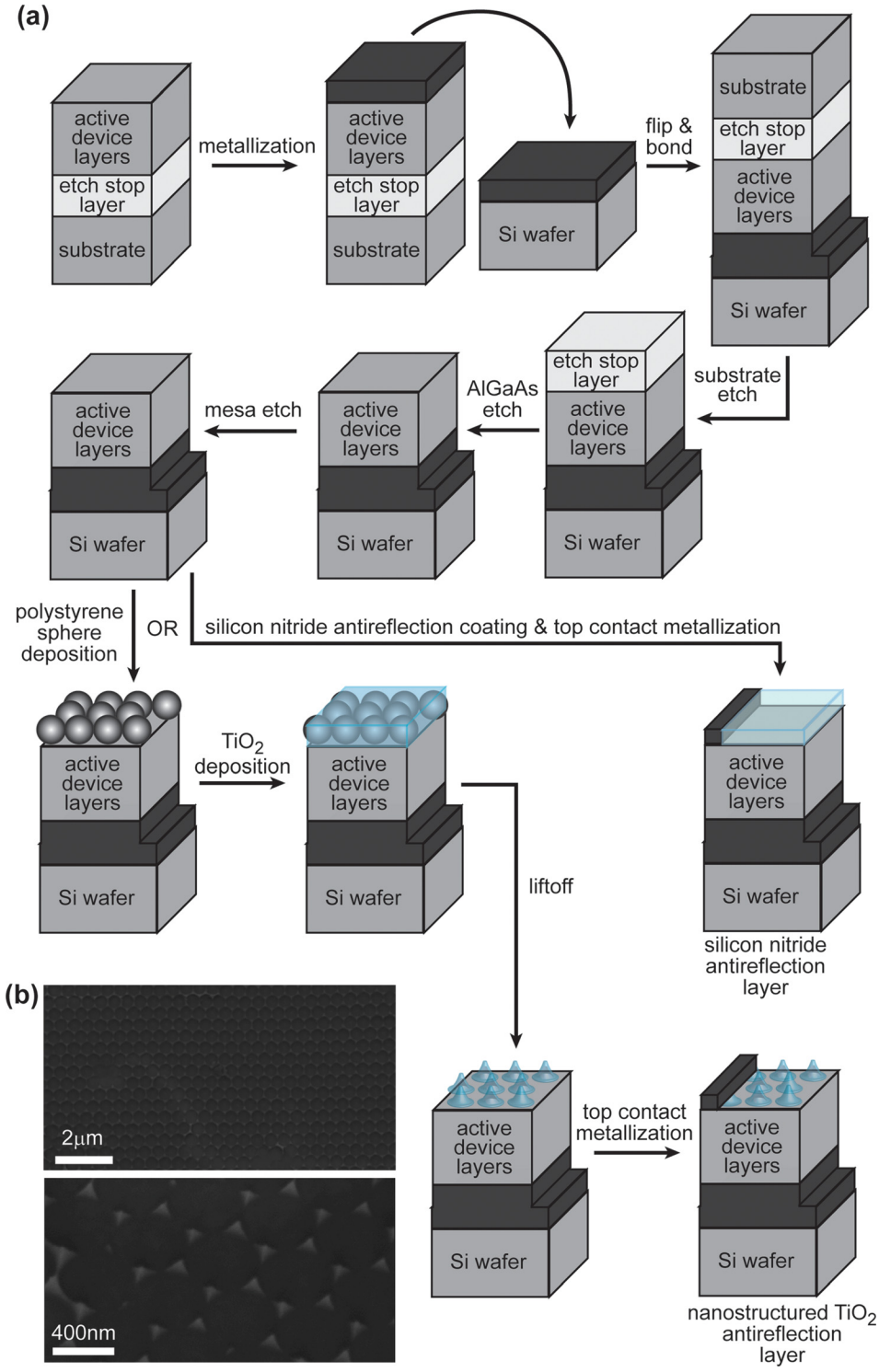

FIG. 2. (a) Key steps in process flow for fabrication of solar cell devices with either silicon nitride thin-film antireflection coating or nanostructured TiO_2 antireflection layer, the latter using nanosphere lithography for patterning. (b) Scanning electron micrograph of nanostructured TiO_2 antireflection layer on GaAs surface. Scale bar is 1 μm.

and simulated E.Q.E. spectra, while at longer wavelengths, the measured and simulated E.Q.E. is generally highest with the nanostructured TiO_2 antireflection coating.

In comparing the measured and simulated E.Q.E. spectra, we note that since surface carrier recombination is neglected in the simulations, the differences between the measured and simulated spectra at wavelengths longer than the GaAs band gap at ~850 nm are due primarily to surface recombination in the measurements. Rough numerical estimates based on a standard drift-diffusion analysis accounting for nonradiative surface recombination[25] indicate that the difference between the simulated and measured spectra in this wavelength range can be accounted for by a GaAs surface recombination velocity of $\sim 10^6$ cm/s, a reasonable value given the dopant concentration of 2.5×10^{18} cm^{-3} at the device surface.[26] At wavelengths of ~700–850 nm, oscillations in the simulated E.Q.E. with wavelength are observed, which arise from Fabry-Perot resonances within the solar cell at wavelengths for which the device thickness is smaller than the absorption depth. These features are observed in the measured E.Q.E. for all three device types at wavelengths of ~750–900 nm.

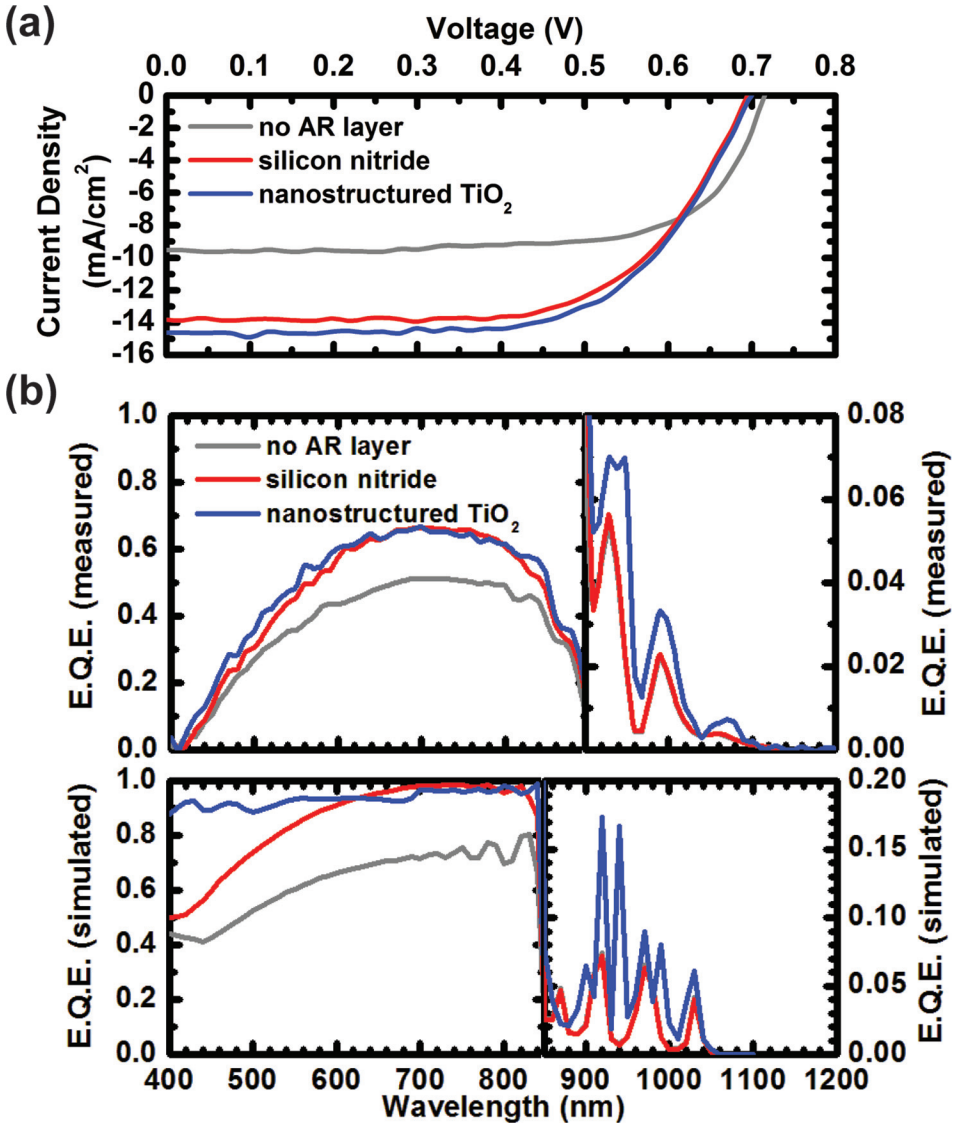

FIG. 3. (a) Current density-voltage characteristics measured under AM1.5G 1-sun illumination from a solar simulator for quantum-well solar cells with no antireflection coating, a silicon nitride thin-film antireflection coating, and a nanostructured TiO_2 antireflection layer. (b) Measured and simulated external quantum efficiency (E.Q.E.) for all three device types.

At wavelengths of ~900 nm or longer, for which optical absorption occurs only in the quantum wells, several peaks are observed in both the measured and simulated E.Q.E. spectra. In this wavelength range, E.Q.E. for devices with either no antireflection layer or a single-layer silicon nitride antireflection coating are indistinguishable from each other, in both measurement and simulation. The peaks observed in the measured spectra at 930 nm, 990 nm, and 1060 nm, and in the simulated spectra at 920 nm, 970 nm, and 1030 nm arise from Fabry-Perot resonances in the device that enable increased quantum-well optical absorption. Similar behavior has been observed previously in quantum-well solar cells grown atop distributed Bragg reflector multilayers.[27] Furthermore, we observe that in both simulation and experiment, the presence of the single-layer antireflection coating has a negligible effect on the Fabry-Perot resonances, as anticipated based on the low reflectivity at the solar cell-air interface. For the device with the nanostructured TiO_2 antireflection layer, however, significantly different behavior is observed. This device exhibits substantially higher measured and simulated E.Q.E at wavelengths longer than 900 nm than the other device types, with a contribution to $J_{sc,th}$, integrated over wavelengths longer than 900 nm, ~1.8 times that for the other devices. Furthermore, there is additional structure in the experimental E.Q.E. spectrum for this device that is not present for the other device types. The simulated E.Q.E. spectrum contains peaks at 920 nm, 970 nm, and 1030 nm—the same wavelengths at which peaks in simulated E.Q.E. are observed for the other device types—and in addition at 900 nm, 940 nm, and 990 nm.

Figure 4 shows simulated electric fields for light incident on solar cell devices with either a single-layer silicon nitride or a nanostructured TiO_2 antireflection coating at wavelengths of 970 nm and 990 nm, with the incident electric field polarized along the y direction. At 970 nm, the electric fields in the semiconductor are predominantly along the y direction for devices with both types of antireflection coatings, indicating that in both cases the enhancement in simulated E.Q.E. at 970 nm is associated with a Fabry-Perot resonance. With the nanostructured antireflection coating, the variation along the y direction in E_y and the nonzero amplitude for E_z at 970 nm, shown in Figure 4(c), arises from scattering by the array of TiO_2 structures. A similar analysis has confirmed that the simulated E.Q.E. peaks at 920 nm and

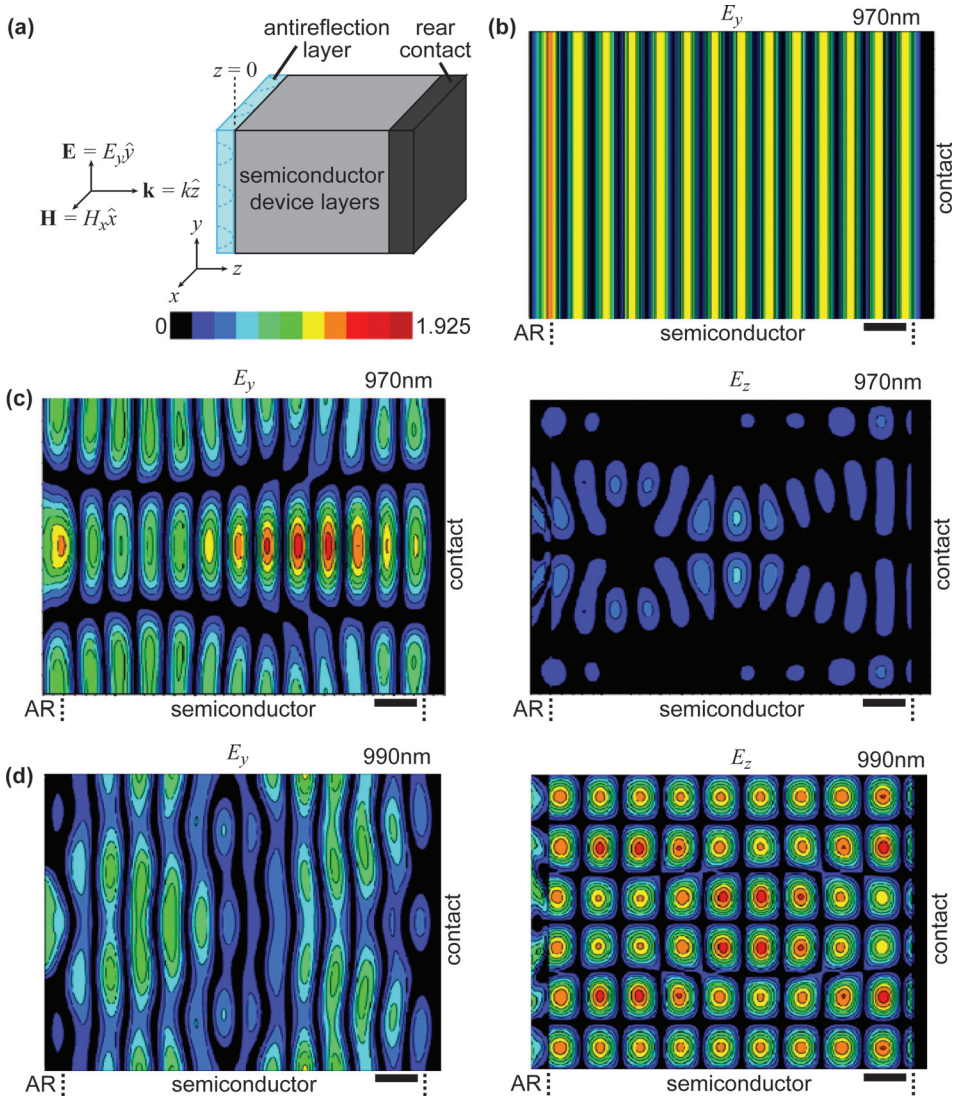

FIG. 4. (a) Schematic diagram of incident field and device geometry for simulations. (b)–(d) Plots of simulated electric field distributions for light incident on quantum-well solar cells with either a silicon nitride thin-film antireflection coating or nanostructured TiO_2 antireflection layer at 970 nm or 990 nm, with the incident electric field polarized along the y direction. (b) E_y at 970 nm for cell with silicon nitride; E_z is negligible in this situation. (c) E_y and E_z at 970 nm for cell with nanostructured TiO_2; (d) E_y and E_z at 990 nm for cell with nanostructured TiO_2. Scale bar for all field plots is 200 nm.

1030 nm for both device types arise from Fabry-Perot resonances. At 990 nm, Figure 4(d) shows that the electric field in the semiconductor in the device with the nanostructured TiO_2 antireflection coating is primarily in the z direction, indicating that at this wavelength the incident light is strongly scattered into a guided optical mode and propagates in a direction orthogonal to that of the incident light. A similar analysis has confirmed that the simulated E.Q.E. peaks at 900 nm and 940 nm for the device with a nanostructured TiO_2 antireflection coating arise from similar scattering behavior. In the measured E.Q.E. spectrum for the device with the nanostructured TiO_2 antireflection coating, two closely spaced peaks are observed at 930–950 nm, which we interpret as corresponding to a combination of the Fabry-Perot and guided-mode simulated peaks at 920 nm and 940 nm. Additional peaks in the measured E.Q.E. spectrum are present at 990 nm and 1070 nm, with the former interpreted as corresponding to a combination of Fabry-Perot and guided-mode simulated peaks at 970 nm and 990 nm, and the latter to the simulated Fabry-Perot peak at 1030 nm. The measured peaks are generally lower in amplitude, but broader, than the simulated peaks, an unsurprising consequence of differences between the actual and simulated structures, and fabrication-induced variations and imperfections in the former.

Because of high surface recombination in these devices, the effects of the nanostructured TiO_2 antireflection coating on short-circuit current density are somewhat suppressed in the current density-voltage measurements shown in Figure 3. An estimate of the potential improvement in short-circuit current density with reduced surface recombination can be obtained by computing $J_{sc,th}$ with the simulated E.Q.E. spectrum shown in Figure 3(c). Such a computation yields values for $J_{sc,th}$ of 30.86 mA/cm^2 and 34.89 mA/cm^2 for devices with thin-film silicon nitride and nanostructured TiO_2 antireflection coatings, respectively.

The nanostructured TiO_2 antireflection layer is also expected to provide low surface reflectivity that persists over a broad range of wavelengths and incident angles.[20–22] Figure 5 shows simulated photocurrent response spectra for quantum-well solar cell device structures with either a thin-film silicon nitride or a nanostructured TiO_2 antireflection coating, for light incident at angles of 20°, 40°, and 60° off normal incidence. Simulated photocurrent response spectra for normally incident illumination were shown in Figure 3(b). The incident light is taken to include s-polarized and p-polarized components with equal amplitudes. As shown in

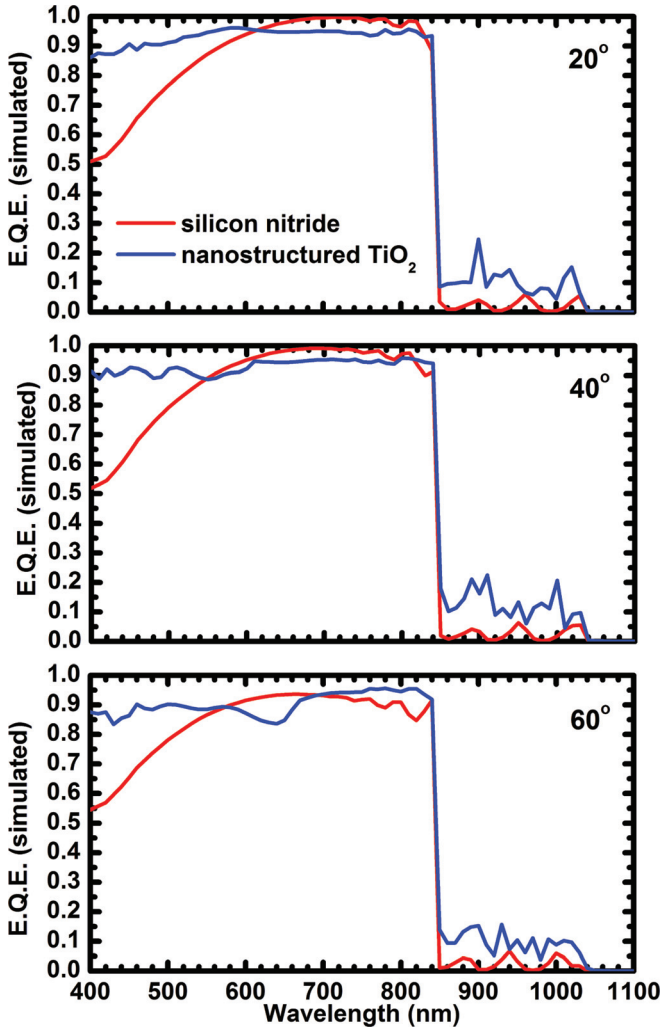

FIG. 5. Simulated external quantum efficiency (E.Q.E.) for device structures with silicon nitride thin-film antireflection coating (red) or nanostructured TiO_2 antireflection layer (blue), as functions of wavelength and computed for incident light polarization at the midpoint (45°) between s-polarization and p-polarization.

Figure 5, the simulated photocurrent response for both structures changes relatively little with increasing angle of incidence for wavelengths shorter than the GaAs band edge at ~850 nm. For the device with a thin-film silicon nitride antireflection coating, this occurs because the increase in surface reflectivity of s-polarized light with increasing incident angle is partially cancelled by the decreased surface reflectivity of p-polarized light as Brewster's angle is approached. At wavelengths below ~600 nm, the reduced reflectivity and higher simulated photocurrent response of the device with the nanostructured TiO_2 antireflection coating, compared to that for the device with a silicon nitride thin-film coating, persists as the angle of incidence is increased. For wavelengths between ~600 nm and ~850 nm, both structures yield generally similar levels of photocurrent response. At wavelengths longer than ~850 nm, for which optical absorption in these simulations occurs only in the quantum wells, the main consequence of increasing angle of incidence for the device with a thin-film silicon nitride antireflection coating is a shift to shorter wavelength, with little change in amplitude, of the photocurrent response peak associated with each Fabry-Perot resonance. For the device with a nanostructured TiO_2 antireflection coating, we observe that the coupling of incident light to optically guided modes improves for off-normal incidence, leading to a substantial increase in expected long-wavelength photocurrent response compared to that for normally incident illumination. This observation could have significant consequences for the efficacy of light trapping approaches in applications for which sunlight is expected to be incident over a broad range of angles.

IV. SUMMARY

In summary, we have characterized and analyzed thin-film solar cells in which a nanostructured TiO_2 antireflection coating fabricated on the top surface using a simple nanosphere lithography patterning process has been shown to provide both superior antireflection performance compared to a conventional single-layer thin-film antireflection coating and scattering of long-wavelength light into guided modes within the solar cell. Implementation of this concept in a quantum-well solar cell allows the influence of the nanostructured TiO_2 layer on light trapping to be elucidated in detail. Measurements demonstrate that the nanostructured TiO_2 antireflection layer yields an increase in J_{sc} of ~5.8% compared to that for an identical solar cell with a conventional single-layer silicon nitride antireflection coating, even in the presence of high surface recombination. Numerical simulations indicate that in the absence of surface recombination, an increase in short-circuit current density of 13% should be attainable. Furthermore, these benefits are shown to persist for illumination incident over a broad range of angles, as one would expect to encounter in a variety of photovoltaic systems.

ACKNOWLEDGMENTS

X.H.L. gratefully acknowledges helpful discussions with Dr. Katsuaki Tanabe for the substrate removal process and part of the device testing work. Part of this work was supported by NSF (ECCS-1128682 and ECCS-1120823) and the Judson S. Swearingen Regents Chair in Engineering at the University of Texas at Austin.

[1]M. A. Green and S. Pillai, Nature Photon. **6**, 130–132 (2012).
[2]P. Campbell and M. A. Green, J. Appl. Phys. **62**, 243 (1987).
[3]Z. Yu, A. Raman, and S. Fan, Proc. Natl. Acad. Sci. U. S. A. **107**, 17491 (2010).
[4]H. A. Atwater and A. Polman, Nature. Mater. **9**, 205 (2010).
[5]E. T. Yu and J. van de Lagemaat, MRS Bull. **36**, 424 (2011).
[6]C. O. McPheeters, D. Hu, D. M. Schaadt, and E. T. Yu, J. Opt. **14**, 024007 (2012).
[7]C. O. McPheeters and E. T. Yu, Opt. Express **20**, A864 (2012).
[8]S. Mokkapati and K. R. Catchpole, J. Appl. Phys. **112**, 101101 (2012).
[9]Y.-F. Huang, S. Chattopadhyay, Y.-J. Jen, C.-Y. Peng, T.-A. Liu, Y.-K. Hsu, C.-L. Pan, H.-C. Lo, C.-H. Hsu, Y.-H. Chang, C.-S. Lee, K.-H. Chen, and L.-C. Chen, Nat. Nanotechnol. **2**, 770 (2007).
[10]W. L. Min, A. P. Betancourt, P. Jiang, and B. Jiang, Appl. Phys. Lett. **92**, 141109 (2008).
[11]E. Garnett and P. Yang, Nano Lett. **10**, 1082 (2010).
[12]N. Yamada, T. Ijiro, E. Okamoto, K. Hayashi, and H. Masuda, Opt. Express **19**, A118 (2011).
[13]P. Yu, M. Y. Chiu, C. H. Chang, C. Y. Hong, Y. L. Tsai, H. V. Han, and Y. R. Wu, "Towards high-efficiency multi-junction solar cells with biologically inspired nanosurfaces," Prog. Photovoltaics. (published online).

[14]J. N. Munday and H. A. Atwater, Nano Lett. **11**, 2195–2201 (2011).
[15]J. J. Schermer, G. J. Bauhuis, P. Mulder, E. J. Havercamp, J. van Deelen, A. T. J. van Niftrik, and P. K. Larsen, Thin Solid Films **511–512**, 645 (2006).
[16]H. Okamoto and T. B. Massalski, *Binary Alloy Phase Diagrams*, edited by T. B. Massalski (ASM International, 1990), p. 381.
[17]K. Tanabe, K. Watanabe, and Y. Arakawa, Appl. Phys. Lett. **100**, 192102 (2012).
[18]C. L. Haynes, A. D. McFarland, M. T. Smith, J. C. Hulteen, and R. P. Van Duyne, J. Phys. Chem. B **106**, 1898 (2002).
[19]J. Rybczynski, U. Ebels, and M. Giersig, Colloids Surf. **219**, 1 (2003).
[20]E. D. Palik, *Handbook of Optical Constants of Solids* (Academic Press, New York, 1998).
[21]S. R. Forrest, MRS Bull. **30**, 28 (2005).
[22]S. Chhajed, M. F. Schubert, J. K. Kim, and E. F. Schubert, Appl. Phys. Lett. **93**, 251108 (2008).
[23]W. H. Southwell, J. Opt. Soc. Am. **8**, 549 (1991).
[24]C. H. Sun, W. L. Min, C. H. Lin, P. Jiang, and B. Jiang, Appl. Phys. Lett. **91**, 231105 (2007).
[25]S. M. Sze, *Physics of Semiconductor Devices* (John Wiley & Sons, New York, 1981), pp. 800–805.
[26]L. Jastrzebski, J. Lagowski, and H. C. Gatos, Appl. Phys. Lett. **27**, 537 (1975).
[27]D. B. Bushnell, N. J. Ekins-Daukes, K. W. J. Barnham, J. P. Connolly, J. S. Roberts, G. Hill, R. Airey, and M. Mazzer, Sol. Energy Mater. Sol. Cells. **75**, 299 (2003).